PERGAMON

Engineering Fracture Mechanics 70 (2003) 29–48

Engineering Fracture Mechanics

www.elsevier.com/locate/engfracmech

Extended finite element method and fast marching method for three-dimensional fatigue crack propagation

N. Sukumar [a,*], D.L. Chopp [b], B. Moran [c]

[a] Department of Civil and Environmental Engineering, University of California, One Shields Avenue, Davis, CA 95616, USA
[b] Department of Engineering Sciences and Applied Mathematics, Northwestern University, Evanston, IL 60208, USA
[c] Department of Civil Engineering, Northwestern University, Evanston, IL 60208, USA

Received 19 June 2001; received in revised form 24 October 2001; accepted 2 January 2002

Abstract

A numerical technique for planar three-dimensional fatigue crack growth simulations is proposed. The new technique couples the extended finite element method (X-FEM) to the fast marching method (FMM). In the X-FEM, a discontinuous function and the two-dimensional asymptotic crack-tip displacement fields are added to the finite element approximation to account for the crack using the notion of partition of unity. This enables the domain to be modeled by finite elements with no explicit meshing of the crack surfaces. The initial crack geometry is represented by level set functions, and subsequently signed distance functions are used to compute the enrichment functions that appear in the displacement-based finite element approximation. The FMM in conjunction with the Paris crack growth law is used to advance the crack front. Stress intensity factors for planar three-dimensional cracks are computed, and fatigue crack growth simulations for planar cracks are presented. Good agreement between the numerical results and theory is realized.

Keywords: Crack propagation; Stress intensity factor; Extended finite element method; Level set method; Fast marching method

1. Introduction

The assessment of fracture and failure of structural components through numerical models remains a challenging problem in computational mechanics. With current thrusts in simulation-based design and damage tolerant assessment of safety-critical aircraft components, the accurate evaluation of fracture parameters such as the stress intensity factor (SIF) for three-dimensional cracked bodies becomes a necessity. Closed-form solutions for the SIFs are available for simple crack geometries in three-dimensions; however, for arbitrary-shaped cracks in finite-specimens, numerical methods are the only recourse to modeling three-dimensional fatigue crack growth.

* Corresponding author. Tel.: +1-530-754-6415; fax: +1-530-752-7872.
E-mail address: nsukumar@ucdavis.edu (N. Sukumar).

0013-7944/03/$ - see front matter
PII: S0013-7944(02)00032-2

Finite element methods are widely used in linear elastic fracture mechanics. In spite of the successes using finite elements in computational fracture, mesh generation in three-dimensions for crack growth simulations is still a formidable task. This is so since to capture the evolution of the crack in fatigue growth, remeshing along with local refinements in the vicinity of the crack front are required to obtain accurate solutions for fracture parameters such as the SIF.

Currently, there are very few numerical tools for three-dimensional fatigue crack growth simulations. Among them, the finite element and boundary element methods [5,9,12,18], the finite element alternating method [22,35], and the dislocation distribution approach [8,15] are prominent. Xu and Ortiz [37] modeled three-dimensional cracks as a continuous distribution of dislocation loops within a variational framework, and used the technique to model non-planar crack growth under mixed mode loading conditions [36]. Within the realm of mesh-free methods, dynamic crack propagation in three-dimensions has been pursued by Krysl and Belytschko [17].

The extended finite element method (X-FEM) alleviates shortcomings associated with the meshing of crack surfaces in existing methods. In this method, the finite element approximation is enriched by additional functions through the notion of partition of unity [19]. Strouboulis et al. [30] have used the partition of unity framework to model holes and cracks in two-dimensions, whereas Duarte et al. [11] have studied the simulation of three-dimensional dynamic crack propagation. For crack modeling in the X-FEM, a discontinuous function and the two-dimensional asymptotic crack-tip displacement fields are added to the displacement-based finite element approximation [20].

The level set framework, and in particular the fast marching method (FMM) provide a seamless means to evolve an interface (crack front). This technique obviates the need to represent and maintain the geometry of the crack during its evolution. The level set method is a numerical technique for tracking moving interfaces [23]. The related FMM [26] is a computationally attractive alternative for strictly monotonically advancing fronts. In both methods, the evolving interface is represented as a level contour of a function of one higher dimension (i.e., $\Psi(\mathbf{x},t) = C$). In the FMM, the motion of the interface is embedded in the solution of an elliptic equation in terms of $\Psi(\mathbf{x},t)$. Crack growth modeling of two-dimensional cracks by coupling the level set description with the X-FEM appears in [29]. Other works that have used the level set method for material interfaces within the context of a mesh-independent Galerkin formulation can be found in [24,32].

In this paper, we propose a novel paradigm for modeling planar three-dimensional cracks and the ability to carry out fatigue crack growth along planar surfaces. The new technique involves the nexus of the X-FEM to the FMM, which results in a powerful numerical tool for crack modeling. The X-FEM and the FMMs are introduced in Sections 2 and 3, respectively. Some of the essentials of three-dimensional crack modeling in the X-FEM are discussed in Section 4. For fatigue crack growth simulations, a second-order upwind finite difference scheme is adopted in the FMM. The governing equations and the weak form for elastostatics are given in Section 5. In Section 6, numerical results for benchmark problems in three-dimensional elastostatics and fatigue crack growth simulations are presented, followed by some concluding remarks in Section 7.

2. Extended finite element method

The X-FEM attempts to alleviate the computational challenges associated with mesh generation by not requiring the finite element mesh to conform to cracks, and in addition, provides a means to use higher-order elements or special finite elements without significant changes in the formulation. Building on prior work due to Belytschko and Black [2], the foundations of the method were presented in [20] for two-dimensional cracks and extended for three-dimensional cracks in [33].

The essence of the X-FEM lies in sub-dividing a model problem into two distinct parts: mesh generation for the geometric domain (cracks and holes not included), and enriching the finite element approximation by additional functions that model the flaw(s) and other geometric entities.

The enrichment of the finite element approximation follows. Consider a point $\mathbf{x}$ of $\mathbb{R}^3$ that lies inside a finite element e. Denote the nodal set $\mathbf{N} = \{n_1, n_2, \ldots, n_m\}$, where m is the number of nodes of element e ($m = 4$ for a constant-strain tetrahedron, $m = 8$ for a trilinear hexahedral element, etc.). The enriched displacement approximation for a vector-valued function $\mathbf{u}(\mathbf{x}) : \mathbb{R}^3 \to \mathbb{R}^3$ assumes the form:

$$\mathbf{u}^h(\mathbf{x}) = \underbrace{\sum_{\substack{I \\ n_I \in \mathbf{N}}} \phi_I(\mathbf{x})\mathbf{u}_I}_{\text{classical}} + \underbrace{\sum_{\substack{J \\ n_J \in \mathbf{N}^g}} \phi_J(\mathbf{x})\psi(\mathbf{x})\mathbf{a}_J}_{\text{enriched}}, \quad (\mathbf{u}_I, \mathbf{a}_J \in \mathbb{R}^3), \tag{1}$$

where the nodal set $\mathbf{N}^g$ is defined as

$$\mathbf{N}^g = \{n_J : n_J \in \mathbf{N}, \omega_J \cap \Omega_g \neq \emptyset\}. \tag{2}$$

In the above equation, $\omega_J = \text{supp}(n_J)$ is the support of the nodal shape function $\phi_J(\mathbf{x})$, which consists of the union of all elements with n_J as one of its vertices, and Ω_g is the domain associated with a geometric entity such as a void, crack surface, or crack front. In general, the choice of the enrichment function $\psi(\mathbf{x})$ that appears in Eq. (1) depends on the geometric entity.

3. Fast marching method

The level set method is a numerical technique for tracking moving interfaces [23]. The related FMM, which is computationally attractive for monotonically advancing fronts, was first introduced by Sethian [26], and later improved by Sethian [27] and Chopp [6]. The key advantages of these methods are that they rely on a fixed Eulerian mesh, handle topological changes in the interface naturally, and can be easily formulated in higher dimensions; see [28] for the many applications of these methods in engineering and the applied sciences. We first describe some basic elements of level set descriptions, and then discuss the details of the FMM algorithm that we use in our computations.

In keeping with the planar three-dimensional crack applications pursued in this paper, we consider the representation of a one-dimensional curve (crack front) on a planar surface in $\mathbb{R}^3$. A moving interface $\Gamma(t)$ can be formulated as the zero level curve of a scalar-valued function $\Psi : \mathbb{R}^2 \times \mathbb{R} \to \mathbb{R}$, where

$$\Gamma(t) = \{\mathbf{x} \in \mathbb{R}^2 : \Psi(\mathbf{x}, t) = 0\}. \tag{3}$$

One important example of such a level set function Ψ would be the signed distance function:

$$\varphi(\mathbf{x}, t) = \pm \min_{\mathbf{x}_\Gamma \in \Gamma(t)} \|\mathbf{x} - \mathbf{x}_\Gamma\|, \tag{4}$$

where the sign is positive (negative) if $\mathbf{x}$ is outside (inside) the contour defined by $\Gamma(t)$. We assume that the interface $\Gamma(t)$ is such that one can define an interior and an exterior to it. As the name suggests, for a given point $\mathbf{x}$, the signed distance function φ attains a value (with the appropriate sign) that is equal to the length of the orthogonal projection (shortest distance) from the point $\mathbf{x}$ to the interface $\Gamma(t)$. For an elliptical interface (crack) located on the x_1–x_2 plane, a level set function is

$$\Psi = \frac{x_1^2}{a^2} + \frac{x_2^2}{b^2} - 1. \tag{5}$$

Note that Ψ is a level set function, but not a signed distance function. In order to obtain the signed distance function φ for an elliptical crack, one applies the FMM to Eq. (6) with $F(\mathbf{x}) = 1$ and the condition (initial interface location) $\varphi^{-1}(0) = \Psi^{-1}(0)$. From hereon, we use Ψ to denote any level set function, whereas φ is used specifically for a signed distance function.

The FMM computes the crossing time map for a monotonically advancing front in an arbitrary number of spatial dimensions. The crossing time map is a function Ψ with the property that $\Psi(\mathbf{x})$ gives the time when a moving front crosses the point $\mathbf{x}$. The crossing time is unique if the front is monotonically advancing. Thus, $\Psi^{-1}(0)$ is the initial position of the front and at any later time t, the front is given by $\Psi^{-1}(t)$. The crossing time map is constructed by solving an equation of the form

$$\|\nabla\Psi(\mathbf{x})\| = \frac{1}{F(\mathbf{x})}, \tag{6}$$

where $F(\mathbf{x})$ is the front speed at the point $\mathbf{x}$. If $F(\mathbf{x}) \equiv 1$, then Eq. (6) becomes the Eikonal equation and the solution $\Psi(\mathbf{x}) \equiv \varphi(\mathbf{x})$ of Eq. (6) gives the distance from $\mathbf{x}$ to the zero contour $\Psi^{-1}(0) = \varphi^{-1}(0)$. We use this method in two ways in this paper: to compute the distance map from the grid nodes to the crack front by using $F \equiv 1$, and to advance the crack front where F represents the computed speed of the crack front.

The FMM solves Eq. (6) by first replacing the gradient by suitable upwind operators, and then systematically advancing the front by marching outwards from the boundary data in an upwind fashion. For N nodes, the method has a total operation count of $O(N \log N)$. In this method, all the nodes in the mesh are sorted into three disjoint sets, the set of all *accepted nodes* A, the set of all *tentative nodes* T, and the set of all *distant nodes* D. The method systematically moves nodes from the set D to the set T and finally into the set A and terminates when all nodes are in the set A. Briefly, the set A consists of all nodes $\mathbf{x}$ whose value of $\Psi(\mathbf{x})$ has been computed, the set T consists of all nodes that are candidates for inclusion into the set A, and the set D consists of all nodes which are too far from the set A to be candidates. With these sets in mind and denoting $\mathbf{x}_{i,j}$ as the coordinate of node (i,j) and $\Psi_{i,j} \equiv \Psi(\mathbf{x}_{i,j})$, the algorithm proceeds as follows:

1. Initialize a core set of nodes to be in the set A. The value of $\Psi(\mathbf{x})$ for $\mathbf{x} \in A$ is determined by direct computation. Each element of the mesh through which the zero contour of Ψ crosses, i.e. the initial front position, has each of its nodes start in the set A and the value of each node is determined by directly computing the distance from each node to the level contour in the element. We use bicubic interpolation on the rectilinear FMM grid to approximate the contour. A variant of Newton's method is used to compute the distance to that contour. For additional details, see Chopp [6].
2. For each node $\mathbf{x} \in A$, each neighboring node $\mathbf{y} \notin A$ connected to $\mathbf{x}$ is assigned a tentative value $\Psi(\mathbf{y})$ and placed in the set T. The tentative value is constructed by using finite difference approximations for Eq. (6). Second-order one-sided finite difference approximations for $\Psi_x(\mathbf{x}_{i,j})$ are given by (see [27])

$$\Psi_x(\mathbf{x}_{i,j}) \approx D_x^- \Psi_{i,j} + \frac{s_1^- \Delta x}{2} D_x^- D_x^- \Psi_{i,j} = \frac{\Psi_{i,j} - \Psi_{i-1,j}}{\Delta x} + \frac{s_1^-}{2}\left(\frac{\Psi_{i,j} - 2\Psi_{i-1,j} + \Psi_{i-2,j}}{\Delta x}\right), \tag{7a}$$

$$\Psi_x(\mathbf{x}_{i,j}) \approx D_x^+ \Psi_{i,j} + \frac{s_1^+ \Delta x}{2} D_x^+ D_x^+ \Psi_{i,j} = \frac{\Psi_{i+1,j} - \Psi_{i,j}}{\Delta x} + \frac{s_1^+}{2}\left(\frac{\Psi_{i,j} - 2\Psi_{i+1,j} + \Psi_{i+2,j}}{\Delta x}\right), \tag{7b}$$

where

$$D_x^- \Psi_{i,j} = \frac{\Psi_{i,j} - \Psi_{i-1,j}}{\Delta x}, \tag{8a}$$

$$D_x^+ \Psi_{i,j} = \frac{\Psi_{i+1,j} - \Psi_{i,j}}{\Delta x}, \tag{8b}$$

and likewise for $D_y^- \Psi_{i,j}$ and $D_y^+ \Psi_{i,j}$. In addition,

$$s_1^- = \begin{cases} 1 & \mathbf{x}_{i-2,j} \in A, \\ 0 & \mathbf{x}_{i-2,j} \notin A, \end{cases} \tag{9a}$$

$$s_1^+ = \begin{cases} 1 & \mathbf{x}_{i+2,j} \in A, \\ 0 & \mathbf{x}_{i+2,j} \notin A, \end{cases} \tag{9b}$$

and likewise for s_2^- and s_2^+.

Similar approximations are used for Ψ_y. Now, if we wish to compute $\Psi_{i,j}$ with $\mathbf{x}_{i-1,j}, \mathbf{x}_{i,j+1} \in A$, then $\Psi_{i,j}$ is constructed by solving the discrete analog of Eq. (6):

$$\left(D_x^- \Psi_{i,j} + \frac{s_1^- \Delta x}{2} D_x^- D_x^- \Psi_{i,j}\right)^2 + \left(D_y^+ \Psi_{i,j} + \frac{s_2^+ \Delta y}{2} D_y^+ D_y^+ \Psi_{i,j}\right)^2 = 1/F_{i,j}^2. \tag{10}$$

Eq. (10) is actually a quadratic in the unknown quantity $\Psi_{i,j}$ and can be solved to produce two possible values. The larger of the two solutions is taken for $\Psi_{i,j}$. A more general form of Eq. (10) with switches for directions is given by [27]

$$\left[\max\left(D_x^- \Psi_{i,j} + \frac{s_1^- \Delta x}{2} D_x^- D_x^- \Psi_{i,j}, -D_x^+ \Psi_{i,j} + \frac{s_1^+ \Delta x}{2} D_x^+ D_x^+ \Psi_{i,j}, 0\right)\right]^2 + \left[\max\left(D_y^- \Psi_{i,j} + \frac{s_2^- \Delta y}{2} D_y^- D_y^- \Psi_{i,j}, -D_y^+ \Psi_{i,j} + \frac{s_2^+ \Delta y}{2} D_y^+ D_y^+ \Psi_{i,j}, 0\right)\right]^2 = 1/F_{i,j}^2. \tag{11}$$

The set T is maintained as a sorted list by a heap sort method with the smallest value always at the top. Pictorially, the set A now consists of all nodes immediately adjacent to the zero contour $\Psi^{-1}(0)$, the set T is a thin layer of nodes surrounding the nodes in A, and the set D is everything else (Fig. 1).

3. The main loop now begins by taking the node $\mathbf{x} \in T$ with the smallest value for $\Psi(\mathbf{x})$ and moves it from the set T to the set A.
4. Each node $\mathbf{y}$ adjacent to the node selected in step 3, and not already in A, has its value $\Psi(\mathbf{y})$ updated using Eq. (11). If $\mathbf{y} \in T$, then T must be re-sorted to account for the changed value of $\Psi(\mathbf{y})$. If $\mathbf{y} \in D$, it is moved from D to T in its correct sorted position.
5. If $T \neq \emptyset$, then go to step 3.

For further information regarding the FMM and the level set method, see [28].

4. Crack modeling

The planar crack is represented by level set functions, and its evolution under fatigue growth conditions is carried out using the FMM. In the earlier three-dimensional implementation of the X-FEM [33], computational geometric issues for the representation of the crack and its interaction with the finite element mesh for the enrichment were discussed. In this paper, geometric issues associated with the crack surface and the evolution of its front are resolved by using level set functions and the FMM.

The crack is modeled by enriching the nodes whose nodal shape function support intersects the interior of the crack by a discontinuous function, and enriching the nodes whose nodal shape function supports intersect the crack front by the two-dimensional asymptotic crack-tip fields. The selection of nodes for enrichment as well as the computation of enrichment functions are carried out by using level set functions. In addition to the above, partitioning algorithms are also implemented if the crack intersects the finite elements [33]. This is required due to the need to accurately integrate (numerically) the weak form, which is achieved by independently integrating the bilinear form on both sides of the crack discontinuity. The partitioned elements for an edge crack that is not aligned with the mesh is shown in Fig. 2. For details on the partitioning algorithm, the interested reader can see [33]; the code is also available in the public-domain [31].

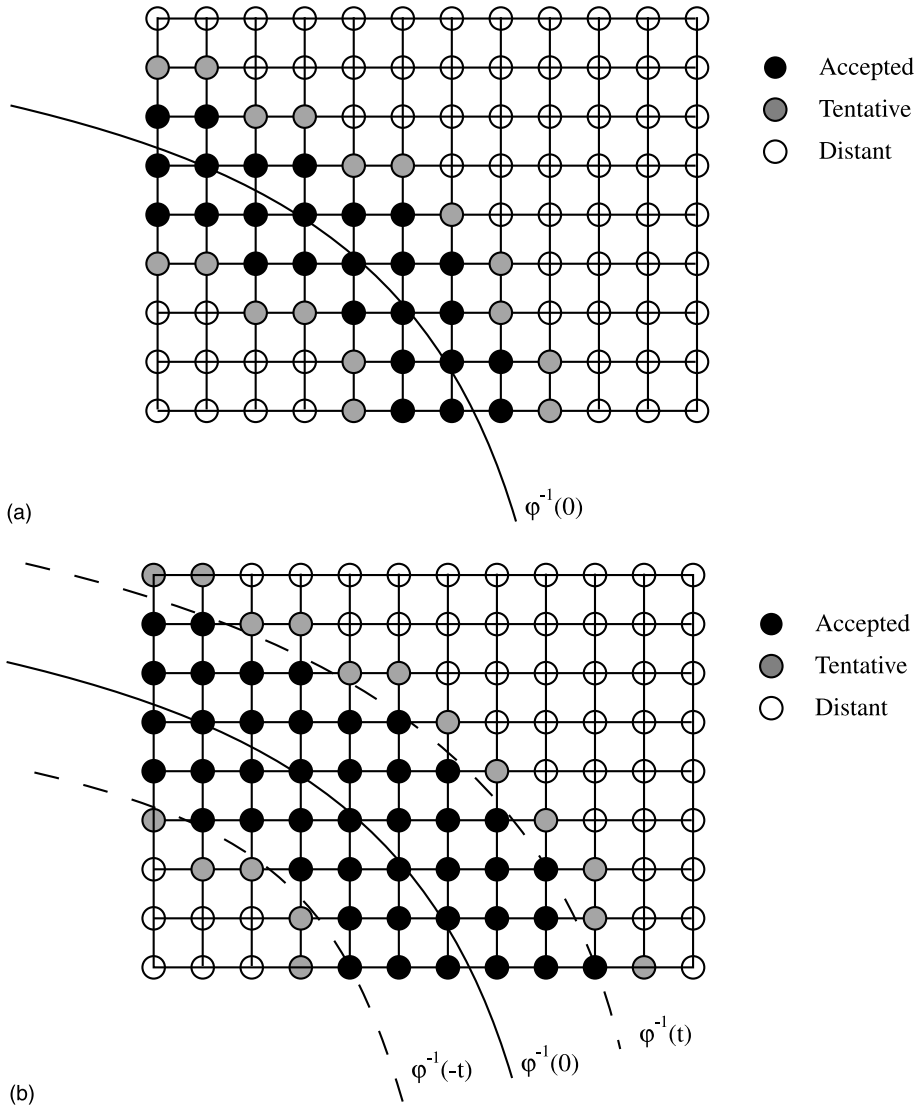

Fig. 1. Nodal sets used in the FMM. (a) Initial step $t = 0$; and (b) intermediate step $t > 0$.

In the following sub-sections, we restrict the description of the implementation to planar cracks (x_1–x_2 plane) in three-dimensions. The extension of the FMM for inclined planar cracks in three-dimensions is straight-forward.

4.1. Enrichment functions

Consider a single crack in three-dimensions, and let Γ_c be the crack surface and Λ_c the crack front. Note that for an internal crack, the crack front corresponds to the boundary of the crack: $\Lambda_c = \partial\Gamma_c$ whereas for an edge crack, the crack front is only part of the boundary: $\Lambda_c \subset \partial\Gamma_c$. The interior of a planar crack is modeled by the enrichment function $H(\mathbf{x})$, which we refer to as a generalized Heaviside function. The

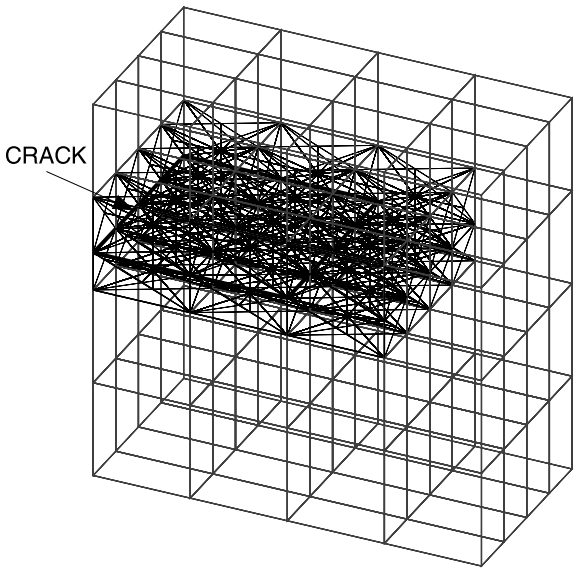

Fig. 2. Element partitioning for an edge-crack within a $4 \times 4 \times 4$ hexahedral mesh.

function $H(\mathbf{x})$ takes on the value $+1$ above the crack and -1 below the crack. More precisely, let $\mathbf{x}^*$ be the closest point to $\mathbf{x}$ on the crack Γ_c, and $\mathbf{n}$ be the normal to the crack plane (Fig. 3). The $H(\mathbf{x})$ function is then given by $+1$ if $(\mathbf{x}-\mathbf{x}^*)\cdot\mathbf{n} \geqslant 0$ and -1 otherwise, i.e.,

$$H(\mathbf{x}) = \begin{cases} 1 & \text{if } (\mathbf{x}-\mathbf{x}^*)\cdot\mathbf{n} \geqslant 0, \\ -1 & \text{otherwise.} \end{cases} \tag{12}$$

To model the crack front and also to improve the representation of crack-tip fields in three-dimensional computations, crack-tip enrichment functions are used in elements which contain the crack front. In the neighborhood of the crack front, the asymptotic fields are two-dimensional in nature. The crack front enrichment consists of functions which incorporate the radial and angular behavior of the two-dimensional asymptotic crack-tip displacement field:

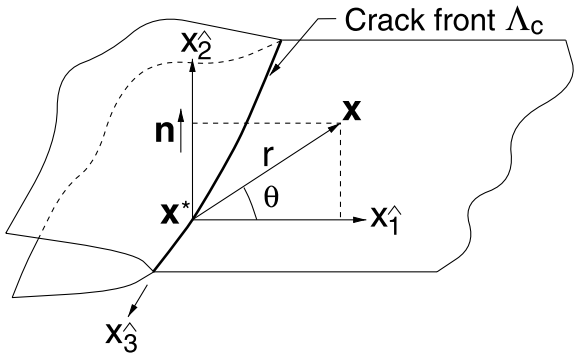

Fig. 3. Coordinate configuration for crack front enrichment functions.

$$\boldsymbol{\Phi}(\mathbf{x}) \equiv \{\psi_1, \psi_2, \psi_3, \psi_4\} = \left[\sqrt{r}\cos\frac{\theta}{2}, \sqrt{r}\sin\frac{\theta}{2}, \sqrt{r}\sin\theta\sin\frac{\theta}{2}, \sqrt{r}\sin\theta\cos\frac{\theta}{2}\right], \tag{13}$$

where r and θ are polar coordinates in the $x_{\hat{1}}$–$x_{\hat{2}}$ plane (Fig. 3). Note that the second function in the above equation is discontinuous on the crack plane.

In order to determine the local coordinate axes $x_{\hat{1}}$–$x_{\hat{2}}$ and the crack interior and crack front enrichment functions, we use signed distance functions φ_1 for the crack front and φ_2 for the crack plane. For the crack interior enrichment, given a point $\mathbf{x}$, $H(\mathbf{x}) = \mathrm{sgn}(\varphi_2(\mathbf{x}))$ is used to compute the generalized Heaviside function given in Eq. (12). In the above, $\mathrm{sgn}(\cdot)$ is the sign function which takes on the value $+1$ if its argument is non-negative, and the value -1 otherwise.

Consider a point $\mathbf{x}$ for which the crack front enrichment functions are to be computed. Let the projection of $\mathbf{x}$ onto the crack plane be $\mathbf{x}_{\mathrm{p}}$. Then, $x_{\hat{1}} = \varphi_1(\mathbf{x}_{\mathrm{p}})$ is the minimum distance to the crack front, and $x_{\hat{2}} = \varphi_2(\mathbf{x})$ is the minimum distance from $\mathbf{x}$ to the crack plane. Using the above, the crack front enrichment functions given in Eq. (13) are computed. In Fig. 4, the level set functions φ_1 and φ_2 are illustrated for a planar crack.

4.2. Selection of enriched nodes

We next describe the enrichment for three-dimensional crack modeling. The enriched finite element approximation is [33]:

$$\mathbf{u}^h(\mathbf{x}) = \sum_{\substack{I \\ n_I \in \mathbf{N}}} \phi_I(\mathbf{x})\mathbf{u}_I + \sum_{\substack{J \\ n_J \in \mathbf{N}^c}} \phi_J(\mathbf{x})H(\mathbf{x})\mathbf{a}_J + \sum_{\substack{K \\ n_K \in \mathbf{N}^f}} \phi_K(\mathbf{x})\left(\sum_{l=1}^{4} \psi_l(\mathbf{x})\mathbf{b}_K^l\right). \tag{14}$$

The second and third terms on the right-hand side of the above equation are the discontinuity and front enrichments, respectively. The set $\mathbf{N}^f$ consists of those nodes for which the closure of the nodal shape

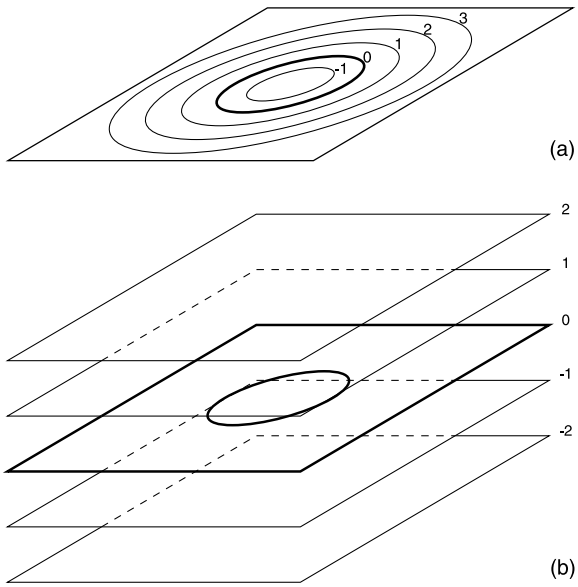

Fig. 4. Level set functions for the crack. (a) φ_1 for the crack front; and (b) φ_2 for the crack plane.

function support intersects the crack front. The set $\mathbf{N}^c$ is the set of nodes whose nodal shape function support is intersected by the crack and which do not belong to $\mathbf{N}^f$:

$$\mathbf{N}^f = \{n_K : n_K \in \mathbf{N}, \bar{\omega}_K \cap \Lambda_c \neq \emptyset\}, \tag{15}$$

$$\mathbf{N}^c = \{n_J : n_J \in \mathbf{N}, \omega_J \cap \Gamma_c \neq \emptyset, n_J \notin \mathbf{N}^f\}. \tag{16}$$

By using the sign of the level set functions φ_1 and φ_2 (see Section 4.1), the nodal sets $\mathbf{N}^c$ and $\mathbf{N}^f$ are easily determined. Note that for any node in $\mathbf{N}^c$, the support of the nodal shape function is fully cut into two disjoint pieces by the crack. If for a certain node n_I, one of the two pieces is very small compared to the other, then the generalized Heaviside function used for the enrichment is almost a constant over the support, leading to an ill-conditioned stiffness matrix [10,20]. Therefore, in this case, node n_I is removed from the set $\mathbf{N}^c$. The criterion for nodal inclusion in $\mathbf{N}^c$ is as follows: The volume above the crack is V_{above}, and the volume below the crack is V_ω^{below}: $V_\omega = V_\omega^{\text{above}} + V_\omega^{\text{below}}$. If either of the two ratios, $V_\omega^{\text{above}}/V_\omega$ or $V_\omega^{\text{below}}/V_\omega$ is below a prescribed tolerance, the node is removed from the set $\mathbf{N}^c$. We use a tolerance $\epsilon = 10^{-4}$.

4.3. Crack growth algorithm

Fatigue crack growth is assumed to be governed by the Paris law (see Section 6.3), with the normal increment Δa computed at discrete points on the crack front. The crack growth algorithm which is adopted follows:

1. Step $t = 0$ ($t_{\max}$ is user-specified). Let Ψ be a level set function for the crack front and φ_1 the signed distance function for the crack front (Fig. 5). Initialize Ψ from the initial crack geometry with $\Psi = 0$ on the crack front, $\Psi < 0$ in the crack interior, and $\Psi > 0$ otherwise. For example, Ψ for an ellipse on the x_1–x_2 plane would be

$$\Psi = \frac{x_1^2}{a^2} + \frac{x_2^2}{b^2} - 1. \tag{17}$$

2. Compute the signed distance function φ_1 using the FMM with $F = 1$:

$$\|\nabla \varphi_1\| = 1, \tag{18}$$

   where $\varphi_1^{-1}(0) = \Psi^{-1}(0)$ describes the crack front (zero level set curve).
3. Evaluate the front speed F at n discrete points on the front. Assuming unit time increment in the FMM, we have $F_i = \Delta a_i$, where Δa_i are computed knowing the SIFs at the n points $\mathbf{x}_i \in \Lambda_c$ ($i = 1, 2, \ldots, n$). See Section 6.3 for details on the evaluation of Δa_i using the Paris growth law. The n points $\mathbf{x}_i$ are chosen to be equally spaced by arc-length around the crack front. The front is easily located by identifying all elements in the two-dimensional level set grid which change sign, then interpolating within the element to get a list of segments forming the front. While locating the front explicitly is sometimes viewed as undesirable in level set methods, it however adds greater flexibility to the method without increasing the overall computational complexity of the method. In this case, it allows for evolving the front where the front speed cannot be directly computed at arbitrary points of the front. This is accomplished by velocity extensions as described in step 4.
4. Given the distance map and a front speed function F defined on the crack front identified by $\varphi_1^{-1}(0)$, a speed function F_{ext} can be computed by solving the equation

$$\nabla F_{\text{ext}} \cdot \nabla \varphi_1 = 0, \tag{19}$$

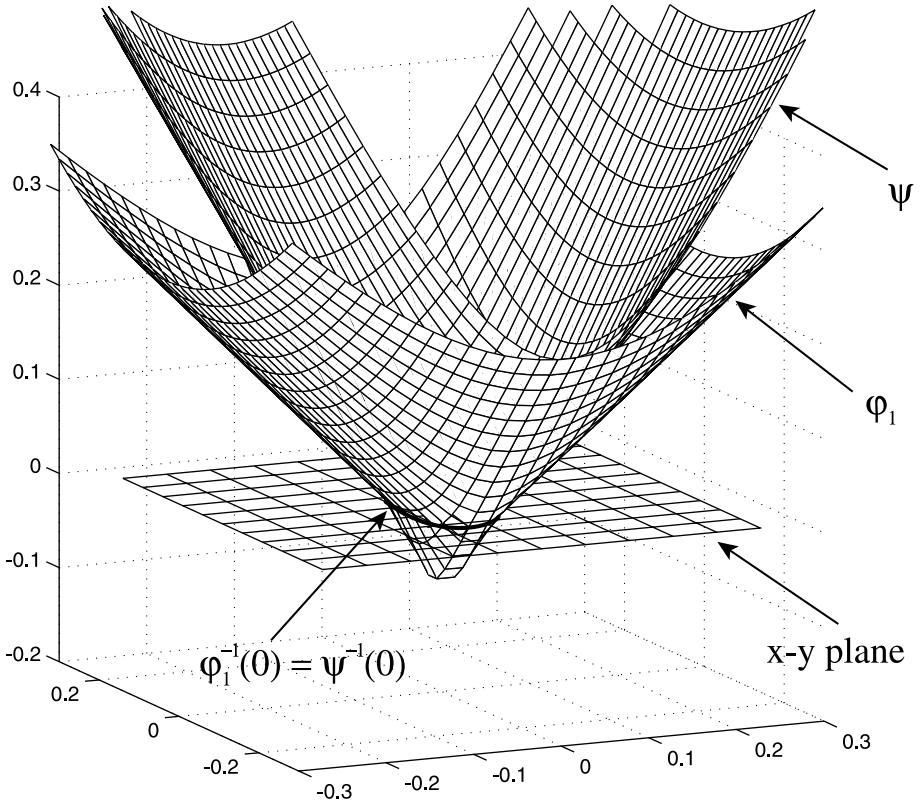

Fig. 5. Level set function (Ψ) and signed distance function (φ_1) for a planar elliptical crack.

where $F_{\text{ext}}|_{\varphi_1^{-1}(0)} = F|_{\varphi_1^{-1}(0)}$ using the FMM [1]. This equation is discretized in the same manner and the nodal values computed in the same order as the FMM. The speed function so constructed is designed so that the speed is constant along lines normal to the crack front.

5. Once F_{ext} is constructed, F_{ext} is inserted into Eq. (6) and the FMM is again applied to compute the crossing time map for the advancing crack front, namely

$$\|\nabla \Psi\| = \frac{1}{F_{\text{ext}}}. \tag{20}$$

Note that the solution Ψ of the above equation is a level set function, but is no longer a distance map. Now, the advancing crack front location at any time Δt later is given by the level curve $\Psi^{-1}(\Delta t)$. The advantage of this technique over a standard level set method approach is that an arbitrarily large time step Δt can be taken without introducing instability and the method is second-order accurate (for convergence tests see [6]). This is ideal for a problem such as crack propagation where computation of the speed is very expensive and accuracy of the distance map φ_1 is critical to obtaining good approximations for the speed.

6. If $t < t_{\max}$, then increment t ($t \leftarrow t + 1$) and go to step 2.

A flowchart that outlines the crack growth algorithm is presented in Fig. 6.

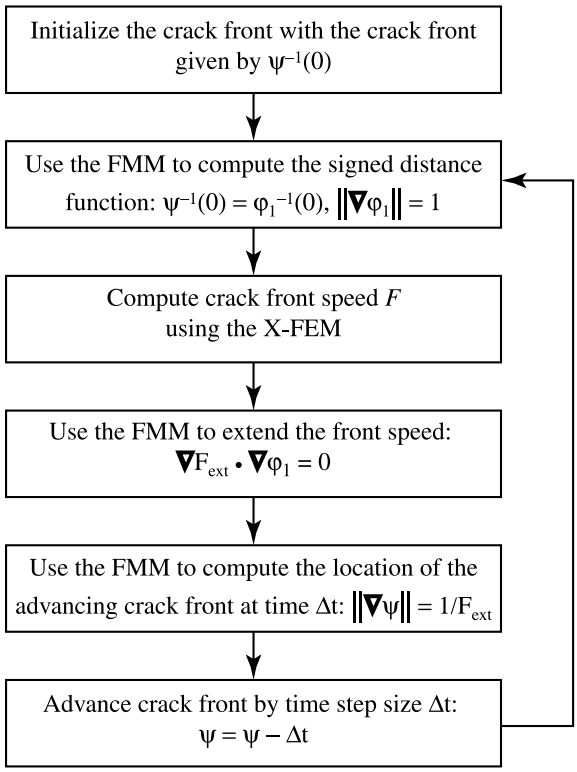

Fig. 6. Flowchart for crack growth algorithm.

5. Governing equations

5.1. Strong form

Consider a body $\Omega \subset \mathbb{R}^3$, with boundary Γ. The boundary Γ consists of the sets Γ_u, Γ_t, and Γ_c^i, such that $\Gamma = \Gamma_u \cup \Gamma_t \cup_{i=1}^m \Gamma_c^i$. All the internal surfaces Γ_c^i are assumed to be traction-free.

The field equations of elastostatics are

$$\nabla \cdot \boldsymbol{\sigma} + \mathbf{b} = 0 \quad \text{in } \Omega, \tag{21a}$$

$$\boldsymbol{\sigma} = \mathbf{C} : \boldsymbol{\varepsilon}, \tag{21b}$$

$$\boldsymbol{\varepsilon} = \nabla_s \mathbf{u}, \tag{21c}$$

where ∇_s is the symmetric gradient operator, $\mathbf{u}$ is the displacement vector, $\boldsymbol{\varepsilon}$ is the small strain tensor, $\boldsymbol{\sigma}$ is the Cauchy stress tensor, $\mathbf{b}$ is the body force vector per unit volume, and $\mathbf{C}$ is the tensor of elastic moduli for a homogeneous isotropic material.

The essential and natural boundary conditions are

$$\mathbf{u} = \bar{\mathbf{u}} \quad \text{on } \Gamma_u, \tag{22a}$$

$$\boldsymbol{\sigma} \cdot \mathbf{n} = \bar{\mathbf{t}} \quad \text{on } \Gamma_t, \tag{22b}$$

$$\boldsymbol{\sigma}\cdot\mathbf{n}=0 \quad \text{on } \Gamma_c^i, \ \ (i=1,2,\ldots,m), \tag{22c}$$

where $\mathbf{n}$ is the unit outward normal to Ω, $\bar{\mathbf{u}}$ and $\bar{\mathbf{t}}$ are prescribed displacements and tractions, respectively, and m is the number of internal surfaces. Note that Eq. (22c) imposes the condition that the internal surfaces Γ_c^i be traction-free.

5.2. Weak form and discrete system

The weak form (principle of virtual work) for linear elastostatics is: Find $\mathbf{u}^h \in \mathbf{V}^h$ such that

$$\int_{\Omega^h}\boldsymbol{\sigma}(\mathbf{u}^h):\boldsymbol{\varepsilon}(\mathbf{v}^h)\,\mathrm{d}\Omega=\int_{\Omega^h}\mathbf{b}\cdot\mathbf{v}^h\,\mathrm{d}\Omega+\int_{\Gamma_t^h}\bar{\mathbf{t}}\cdot\mathbf{v}^h\,\mathrm{d}\Gamma \quad \forall\mathbf{v}^h\in\mathbf{V}_0^h, \tag{23}$$

where $\mathbf{u}^h(\mathbf{x})\in\mathbf{V}^h$ and $\mathbf{v}^h(\mathbf{x})\in\mathbf{V}_0^h$ are the approximating trial and test functions used in the X-FEM. The space $\mathbf{V}^h$ is the enriched finite element space that satisfy the essential boundary conditions, and which include basis functions that are discontinuous across the crack surfaces. The space $\mathbf{V}_0^h$ is the corresponding space with homogeneous essential boundary conditions.

The trial and test functions, which are based on Eq. (14) are

$$\mathbf{u}^h(\mathbf{x})=\sum_{\substack{I\\ n_I\in\mathbf{N}}}\phi_I(\mathbf{x})\mathbf{u}_I+\sum_{\substack{J\\ n_J\in\mathbf{N}^c}}\phi_J(\mathbf{x})H(\mathbf{x})\mathbf{a}_J+\sum_{\substack{K\\ n_K\in\mathbf{N}^f}}\phi_K(\mathbf{x})\left(\sum_{l=1}^{4}\psi_l(\mathbf{x})\mathbf{b}_K^l\right), \tag{24}$$

$$\mathbf{v}^h(\mathbf{x})=\sum_{\substack{I\\ n_I\in\mathbf{N}}}\phi_I(\mathbf{x})\mathbf{v}_I+\sum_{\substack{J\\ n_J\in\mathbf{N}^c}}\phi_J(\mathbf{x})H(\mathbf{x})\mathbf{c}_J+\sum_{\substack{K\\ n_K\in\mathbf{N}^f}}\phi_K(\mathbf{x})\left(\sum_{l=1}^{4}\psi_l(\mathbf{x})\mathbf{e}_K^l\right), \tag{25}$$

where $\phi_I(\mathbf{x})$ are the finite element shape functions, and $\psi_j(\mathbf{x})$ ($j=1$–4) are the enriched functions for the crack front, which are given in Eq. (13).

On substituting the trial and test functions from Eq. (24) in (23), and using the arbitrariness of nodal variations, the discrete linear system $\mathbf{Kd}=\mathbf{f}$ is obtained, which is solved for the unknown vector $\mathbf{d}$. Explicit expressions for the stiffness matrix $\mathbf{K}$ and the external force vector $\mathbf{f}$ can be found in [33].

6. Numerical results

Benchmark three-dimensional planar crack problems and fatigue crack propagation simulations are presented to illustrate the accuracy of the proposed technique. We consider full models (domains and cracks) without utilizing the planes of symmetry since the full model provides a means to assess if the numerical solution can capture the inherent symmetry in the solution-field; however, the proposed technique has no limitations in its applicability to model quarter or one-eighth models by imposing the necessary symmetric essential boundary conditions. In all problems, numerical integration is carried out using Gauss–Legendre quadrature. In hexahedral elements associated with only the finite element shape functions, $2\times2\times2$ quadrature is used, and in elements that also have enriched degrees of freedom, $6\times6\times6$ quadrature is used. The elastic constants used in the computations are: Young's Modulus $E=10^5$ and Poisson's ratio $\nu=0.3$. The numerical implementation is carried out in C++.

6.1. Computation of stress intensity factors

Domain integral methods [21] are used to evaluate SIFs along the three-dimensional crack front. The SIFs for pure mode I crack problems can be evaluated using the domain-form of the contour J-integral; in mixed mode fracture computations where K_{I}, K_{II}, and K_{III} are in general non-zero, the interaction integral formulation is used to extract all the SIFs [13].

For the mode I crack problems considered here, the SIF at a point s on the crack front is given by

$$K_{\mathrm{I}}(s) = \sqrt{\frac{J(s)E}{1-\nu^2}}. \tag{26}$$

With the normal to the crack front (and in the crack plane) oriented along the $\hat{x}_1$-axis of a local coordinate system, the pointwise J-integral is given by

$$J(s) = \lim_{\Gamma \to 0} \int_{\Gamma(s)} H_{\hat{1}\beta} n_\beta \, \mathrm{d}\Gamma, \quad (\beta = \hat{1}, \hat{2}), \tag{27}$$

where

$$H_{\hat{1}j} = W\delta_{\hat{1}j} - \sigma_{ij} u_{i,\hat{1}} \quad (i,j = \hat{1},\ \hat{2},\ \hat{3}). \tag{28}$$

Domain integral representations of the crack-tip contour integral provide a convenient and accurate method for evaluating SIFs in two-dimensional or three-dimensional fracture. For linear elastostatics, in the absence of body forces and material inhomogeneities, and assuming traction-free crack surfaces, the volume form of the domain integral is given by [21]:

$$J(s) = -\frac{\int_V (H_{kj} q_{k,j} + H_{kj,j} q_k) \, \mathrm{d}V}{\int_{L_{\mathrm{c}}} l_k n_k \, \mathrm{d}s}, \tag{29}$$

where V is a volume enclosing the crack front; $n_k(s)$ are components of the in-plane unit outward normal at s; $l_k(s)$ are components of an arbitrary unit vector at s lying in the plane of the crack; and L_{c} is the perturbed segment (virtual extension) along the crack front (Fig. 7). The vector field q_k is defined in V as

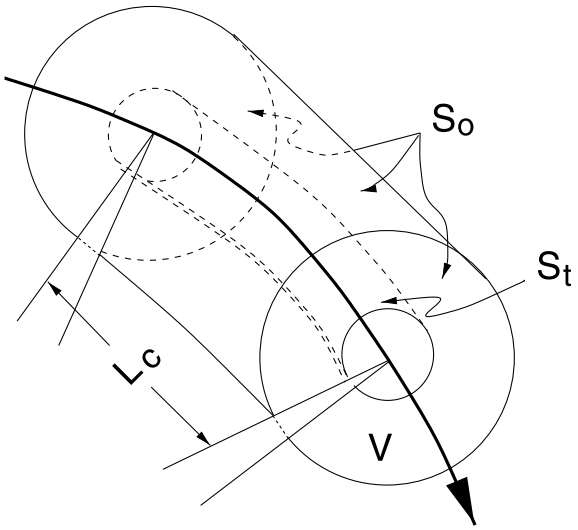

Fig. 7. Volume representation for J-integral evaluation.

$$q_k = \begin{cases} l_k & \text{on } S_t, \\ 0 & \text{on } S_0, \\ \text{arbitrary} & \text{otherwise.} \end{cases} \tag{30}$$

Further details of the three-dimensional implementation of domain integrals in the X-FEM can be found in [33].

As noted earlier, two level set functions are used to model the crack: one to represent the evolving planar crack configuration (φ_1), and the second to represent the crack plane (φ_2). These level set functions are used to locate the nearest point on the crack front associated with a point in the computational domain. This information is required for domain integral computations as well as for computing the enrichment functions. For a planar crack with a parametric representation for its curvilinear front, existing methods for accomplishing this are based on Newton root finding [13]. The level set approach greatly simplifies and speeds-up this task for general crack geometries. In addition, the level set distance functions can also be used to compute the auxiliary fields necessary for the interaction integral in mixed-mode SIF evaluation.

6.2. Benchmark problems

For an infinite domain, two well-known and widely used benchmarks are the penny crack and the elliptical crack under pure mode I loading conditions. We compare the numerical SIFs to the SIF solutions for the above problems.

6.2.1. Planar penny crack in an infinite domain

Let a be the radius of a penny crack with x_3 the coordinate axis normal to the plane of the crack. The closed-form solution for the SIF along the crack front of a penny crack in an infinite domain under uniaxial tension is given by [14,16]:

$$K_{\mathrm{I}}^{E} = 2\sigma_{33}^{0}\sqrt{\frac{a}{\pi}}. \tag{31}$$

Consider a penny crack of radius $a = 0.1$ inside a bi-unit cube. The specimen is subjected to the stress $\sigma_{33}^{0} = 1$ in the x_3-direction. Since the effects of the finite size of the model are minimal, we use the exact solution given in Eq. (31). The finite element mesh used consists of $24 \times 24 \times 24$ hexahedral elements, with graded refinement towards the center of the cube and in the plane of the crack (Fig. 8). The nodes normal to the crack surface are equi-spaced with length $h = 1/12$.

The dimensions of the domain for SIF computations are: $L_{\hat{1}} = a/2$, $L_{\hat{2}} = a/2$, $L_{\hat{3}} = 2a$. The SIF results have four-fold symmetry; hence results for only $0^\circ \leqslant \theta \leqslant 90^\circ$ are presented. In Table 1, the numerical SIF results are presented as a function of θ, and in addition comparisons with the results obtained in the earlier implementation of the X-FEM without the level set representation for cracks [33] are also shown to demonstrate the accuracy of the new technique. The results are observed to be in good agreement with the exact solution: the errors in the SIFs are between 0.4% and 2.9%.

6.2.2. Planar elliptical crack in an infinite domain

We consider an elliptical crack with semi-major axis $a = 0.1$ and semi-minor axis $b = 0.05$ inside a bi-unit cube. The body is subjected to unit tractions $\sigma_{33}^{0} = 1$ on $x_3 = \pm 1$. The coordinate axis x_3 is normal to the plane of the crack. Since the crack-dimensions are small compared to the specimen, we use the infinite domain solution as the reference solution. The exact SIF solution for a planar elliptical crack in an infinite domain is [16]:

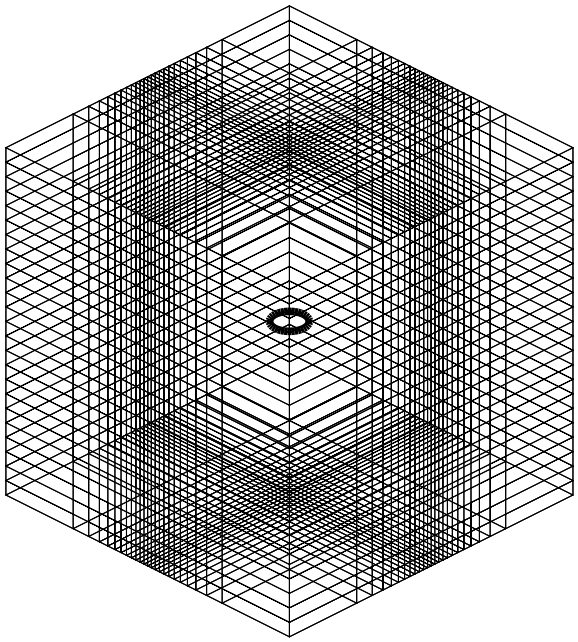

Fig. 8. Surface mesh ($24 \times 24 \times 24$) for a bi-unit cube with an embedded penny crack of radius $a = 0.1$.

Table 1
SIFs for the penny crack problem

θ (deg)	K_{I}^{E}	K_{I} [33]	K_{I}
0	0.3568	0.3508	0.3509
10	0.3568	0.3583	0.3585
20	0.3568	0.3592	0.3590
30	0.3568	0.3467	0.3466
40	0.3568	0.3535	0.3536
50	0.3568	0.3535	0.3536
60	0.3568	0.3467	0.3466
70	0.3568	0.3592	0.3590
80	0.3568	0.3583	0.3585
90	0.3568	0.3508	0.3509

$$K_{\mathrm{I}}^{E} = \frac{\sigma_{33}^{0}\sqrt{\pi b}}{E(k)}\left\{ \sin^2\theta + \frac{b^2}{a^2}\cos^2\theta \right\}^{1/4}, \tag{32}$$

where θ is the elliptic angle (Fig. 9), σ_{33}^{0} is the far-field applied stress in the x_3-direction, and $E(k)$ which is the elliptic integral of the second kind is given by

$$E(k) = \int_0^{\pi/2} \sqrt{1 - k^2 \sin^2\theta}\,\mathrm{d}\theta, \quad k^2 = \frac{a^2 - b^2}{a^2}. \tag{33}$$

The finite element mesh consists of $24 \times 24 \times 24$ hexahedral elements (Fig. 8). The dimensions of the virtual extension domain are: $L_{\hat{1}} = 2b$, $L_{\hat{2}} = b$, $L_{\hat{3}} = 4b$. The SIF results have four-fold symmetry; hence results for only $0^\circ \leqslant \theta \leqslant 90^\circ$ are presented. For the chosen values of a and b, the value of the elliptic integral

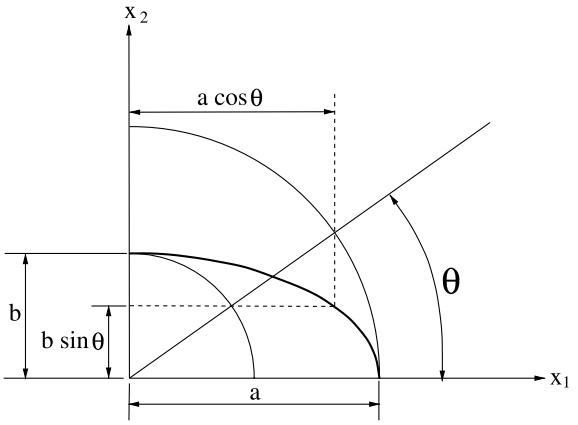

Fig. 9. Geometric definitions for an elliptical crack.

Table 2
SIFs for the elliptical crack problem

θ (deg)	K_{I}^{E}	K_{I} [33]	K_{I}
0	0.2314	0.2358	0.2359
10	0.2365	0.2378	0.2379
20	0.2495	0.2459	0.2461
30	0.2662	0.2564	0.2566
40	0.2830	0.2776	0.2775
50	0.2983	0.2965	0.2960
60	0.3107	0.3089	0.3082
70	0.3198	0.3163	0.3163
80	0.3253	0.3194	0.3193
90	0.3273	0.3202	0.3203

$E(k) = 1.211096$ [4]. In Table 2, the SIF results are presented as a function of the elliptic angle θ. The agreement between the exact solution and the numerical results is good for the entire range of θ. The minimum ($\theta = 10°$) and maximum ($\theta = 30°$) errors in the SIFs are 0.6% and 3.7%, respectively.

6.3. Fatigue crack growth simulations

Fatigue is a common source of failure in structural components that are subjected to cyclical loads, and hence fatigue life predictions play an important role in the damage tolerant assessment of structures. Within the realm of finite element elements, automatic remeshing for crack propagation analysis is the prevailing standard [5], although alternative techniques based on local moving mesh patches are also being explored [25]. The need to remesh at every step and to keep track of the geometry of the evolving crack renders re-meshing techniques to be time-intensive for the analyst. In the new technique for fatigue crack growth simulation proposed herein, no re-meshing is required, geometric issues are greatly simplified by using the level set framework, and a single mesh can be used for fatigue growth of cracks of different shapes and sizes.

We consider planar fatigue crack propagation in three-dimensions. The rate at which the crack grows is governed by Paris law, namely

$$\frac{\mathrm{d}a}{\mathrm{d}N} = C(\Delta K)^m, \tag{34}$$

where C and m are material constants and ΔK is the SIF range. For the mode I problem considered here, we use $\Delta K = K_{\mathrm{I}}$. Let n be the number of points on the crack front at which the SIF is evaluated, and $\Delta a_{\max}$ the maximum user-specified increment normal to the crack front. Then,

$$\frac{\Delta a_i}{\Delta a_{\max}} = \left(\frac{K_{\mathrm{I}}^i}{K_{\mathrm{I}}^{\max}} \right)^m, \tag{35}$$

which gives the normal growth increment at any point $\mathbf{x}_i \in \Lambda_{\mathrm{c}}$ $(i = 1, 2, \ldots, n)$. In the computations, for a user-specified n, the crack front is parameterized by arc length s such that s_t is the total length of the crack front. Then, $\Delta s = s_t/n$ is used as the increment on the crack front to find the coordinates of the n points on the crack front.

In order to test fatigue crack growth simulation, we conduct a simple test that was also adopted in [3,7,8]. Consider a planar elliptical crack embedded in a full space which is subjected to a uniform oscillating (in time) tension σ_{33}^0. Experimental observation indicate that the effects of fatigue smooth out the crack front such that the variation of the SIF along the crack front is minimized. Hence, irrespective of the initial crack geometry, the crack will eventually attain a circular shape, so that K_{I} is constant along the crack front.

We consider an initial elliptical crack of semi-major and semi-minor axes $a = 0.1$ and $b = 0.05$, respectively, which is embedded in a bi-unit cube. The parameters used are: $\Delta a_{\max} = 0.05a$, $m = 2.1$, and $n = 36$. For the FMM, we use a 1000×1000 rectilinear grid with bilinear interpolation in each grid cell. It is to be noted that accuracy considerations in the computation of the enrichment functions (which use the distance map) necessitate such a refined fast marching grid. However, since the fast marching computations form only a fraction of the overall simulation time, the added refinement adds little to the computational costs. The underlying finite element mesh consists of hexahedral elements (Fig. 8). The evolution of the crack front is plotted using bilinear interpolation on the level set grid cells in which there is a zero-crossing. In Fig. 10, the numerical simulation of the crack front evolution is shown for 36 time steps. It is observable that the crack eventually grows to a penny-shape which corroborates experimental observation. In Fig. 11, the ability of the technique to maintain an initial circular front is demonstrated. The fatigue growth simulation of a single penny-shaped crack is compared to the exact solution. There is good agreement between the simulation results and the exact solution, with the crack front remaining nearly circular during its evolution. The parameters used in this case are: $a = 0.05$, $\Delta a_{\max} = 0.2a$, $m = 2.1$, and $n = 36$.

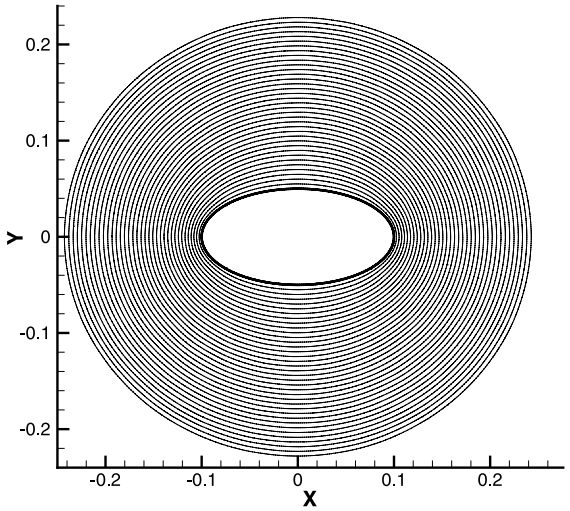

Fig. 10. Fatigue crack growth simulation of an elliptical crack.

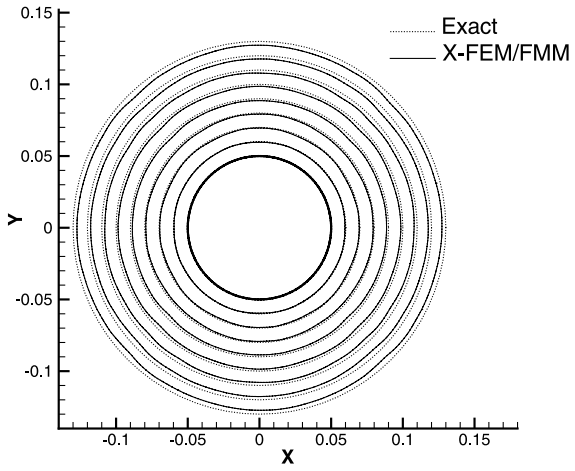

Fig. 11. Fatigue crack growth simulation of a penny-shaped crack.

By using the present technique, a fully automated and accurate fatigue crack growth simulation is carried out without the need to remesh the crack during its evolution. This is in contrast to finite element methods based on re-meshing [5], which engender significant complexity in maintaining and describing the crack geometry during fatigue growth analysis. As opposed to three-dimensional elastostatic fracture computations using the element-free Galerkin (EFG) method [3,34], the X-FEM as a fracture tool appears to provide results that are more robust and accurate for general planar crack geometries.

7. Conclusions

A novel numerical paradigm for three-dimensional crack propagation of planar cracks was proposed. The new technique is based on the nexus of the X-FEM to the FMM. In the X-FEM, the finite element space is enriched by adding special functions to the approximation using the notion of partition of unity. The planar three-dimensional crack was represented by two level set functions: one for the crack front and the other for the crack plane. For three-dimensional crack modeling, a discontinuous function was used to model the interior of the crack surface, and functions from the two-dimensional asymptotic crack-tip displacement fields were used for the crack front enrichment. These enrichment functions were added to the finite element approximation within the context of a displacement-based Galerkin formulation. A second-order upwind finite difference scheme was adopted in the FMM. A computational algorithm for crack growth using the X-FEM and the FMM was also presented.

The performance of the new technique for three-dimensional static cracks was studied. Benchmark mode I problems of penny and elliptical cracks in an infinite domain were solved. The numerical SIFs were found to be in good agreement with the exact solution for these problems. Fatigue crack growth simulations were also carried out. First we studied the growth of an elliptical crack that grew to a circular crack. In addition, we also demonstrated that an initial penny-shaped crack remained circular in shape under fatigue growth.

This study has demonstrated that by combining the X-FEM to the FMM, a powerful and accurate numerical tool emerges for modeling three-dimensional planar cracks. By using a discontinuous (generalized Heaviside) function to model the crack interior [20], the simplicity of the method and the ease of implementation within a finite element framework is readily seen. Enrichment of the displacement field by the two-dimensional asymptotic crack fields [2] accurately models the crack front and also provides good

accuracy for the SIFs on relatively coarse meshes [20,33]. By eliminating the need to include the crack surfaces in the discrete model, mesh generation is greatly simplified; in addition, by using the FMM, a single mesh suffices for fatigue crack growth studies with no user-intervention required during the entire analysis.

Clearly, the coupling of the X-FEM and the FMM has tremendous potential as a simulation tool for a broad range of interfacial phenomena.

Acknowledgements

The authors are grateful for the research support of the National Science Foundation through contract CMS-9732319, the Multi-University Center for Integrated Diagnostics, Georgia Institute of Technology ONR Grant N0014-95-1-0539, the Federal Aviation Administration Grant no. IA025, and the NSF/DARPA VIP program under award 96-15877. The contributions of Nicolas Moës towards the development of the X-FEM are also greatly appreciated.

References

[1] Adalsteinsson D, Sethian JA. The fast construction of extension velocities in level set methods. J Computat Phys 1999;148(1):2–22.
[2] Belytschko T, Black T. Elastic crack growth in finite elements with minimal remeshing. Int J Numer Meth Eng 1999;45(5):601–20.
[3] Black T. Mesh-free applications to fracture mechanics and an analysis of the corrected derivative method, PhD thesis, Theoretical and applied mechanics, Northwestern University, Evanston, IL, USA, 1999.
[4] Byrd RF, Friedman MD. Handbook of elliptic integrals for engineer scientists. Berlin: Springer-Verlag; 1971.
[5] Carter BJ, Wawrzynek PA, Ingraffea AR. Automated 3-d crack growth simulation. Int J Numer Meth Eng 2000;47:229–53.
[6] Chopp DL. Some improvements on the fast marching method. SIAM J Sci Comput 2001;23(1):230–44.
[7] Dai DN, Hills DA. Simulation of the growth of near-surface defects. Eng Fract Mech 1998;59(4):415–24.
[8] Dai DN, Hills DA, Nowell D. Modelling of growth of three-dimensional cracks by a continuous distribution of dislocation loops. Computat Mech 1997;19:538–44.
[9] Dhondt G. Automatic 3-D mode I crack propagation calculations with finite elements. Int J Numer Meth Eng 1998;41(4):739–57.
[10] Dolbow J. An extended finite element method with discontinuous enrichment for applied mechanics. PhD thesis, Theoretical and applied mechanics, Northwestern University, Evanston, IL, USA, 1999.
[11] Duarte CA, Hamzeh ON, Liszka TJ, Tworzydlo WW. The element partition method for the simulation of three-dimensional dynamic crack propagation. Comp Meth Appl Mech Eng 2001;119(15–17):2227–62.
[12] Gerstle WH, Martha L, Ingraffea AR. Finite and boundary element modeling of crack propagation in two- and three-dimensions. Eng Comp 1987;2:167–83.
[13] Gosz M, Dolbow J, Moran B. Domain integral formulation for stress intensity factor computation along curved three-dimensional interface cracks. Int J Solids Struct 1998;35:1763–83.
[14] Green AE, Sneddon IN. The distribution of stress in the neighborhood of a flat elliptical crack in an elastic solid. Proc Camb Philos Soc 1950;47:159–64.
[15] Hills DA, Kelly PA, Dai DN, Korsunsky AM. Solution of crack problems: the distributed dislocation technique. Dordrecht, The Netherlands: Kluwer Academic Publishers; 1996.
[16] Irwin GR. The crack extension force for a part-through crack in a plate. ASME J Appl Mech 1962;29:651–4.
[17] Krysl P, Belytschko T. The element-free Galerkin method for dynamic propagation of arbitrary 3-d cracks. Int J Numer Meth Eng 1999;44(6):767–800.
[18] Martha LF, Wawrzynek PA, Ingraffea AR. Arbitrary crack representation using solid modeling. Eng Comp 1993;9:63–82.
[19] Melenk JM, Babuška I. The partition of unity finite element method basic theory and applications. Comp Meth Appl Mech Eng 1996;139:289–314.
[20] Moës N, Dolbow J, Belytschko T. A finite element method for crack growth without remeshing. Int J Numer Meth Eng 1999;46(1):131–50.
[21] Moran B, Shih CF. Crack tip and associated domain integrals from momentum and energy balance. Eng Fract Mech 1987;27(6):615–41.
[22] Nishioka T, Atluri SN. Analytical solution for embedded cracks, and finite element alternating method for elliptical surface cracks, subjected to arbitrary loading. Eng Fract Mech 1983;17:247–68.

[23] Osher S, Sethian JA. Fronts propagating with curvature-dependent speed: algorithms based on Hamilton–Jacobi formulations. J Computat Phys 1988;79(1):12–49.
[24] Rao VS, Hughes TJR, Garikipati K. On modelling thermal oxidation of silicon II: numerical aspects. Int J Numer Meth Eng 2000;47(1–3):359–77.
[25] Rashid MM. Arbitrary local mesh replacement method: an alternative to remeshing for crack propagation analysis. Comp Meth Appl Mech Eng 1998;154(1–2):133–50.
[26] Sethian JA. A marching level set method for monotonically advancing fronts. Proc Natl Acad Sci 1996;93(4):1591–5.
[27] Sethian JA. Fast marching methods. SIAM Rev 1999;41(2):199–235.
[28] Sethian JA. Level set methods and fast marching methods: evolving interfaces in computational geometry fluid mechanics computer vision and materials science. Cambridge, UK: Cambridge University Press; 1999.
[29] Stolarska M, Chopp DL, Moës N, Belytschko T. Modeling crack growth by level sets and the extended finite element method. Int J Numer Meth Eng 2001;51(8):943–60.
[30] Strouboulis T, Babuška I, Copps K. The design and analysis of the generalized finite element method. Comp Meth Appl Mech Eng 2000;181(1–3):43–69.
[31] Sukumar N. Element partitioning code in 2-d and 3-d for the extended finite element method. Available from http://dilbert.engr.ucdavis.edu/~suku/xfem 2000.
[32] Sukumar N, Chopp DL, Moës N, Belytschko T. Modeling holes and inclusions by level sets in the extended finite element method. Comp Meth Appl Mech Eng 2001;190(46–47):6183–200.
[33] Sukumar N, Moës N, Moran B, Belytschko T. Extended finite element method for three-dimensional crack modeling. Int J Numer Meth Eng 2000;48(11):1549–70.
[34] Sukumar N, Moran B, Black T, Belytschko T. An element-free Galerkin method for three-dimensional fracture mechanics. Computat Mech 1997;20:170–5.
[35] Vijayakumar K, Atluri SN. An embedded elliptical flaw in an infinite solid, subject to arbitrary crack-face tractions. J Appl Mech 1981;48:88–96.
[36] Xu G, Bower AF, Ortiz M. An analysis of non-planar crack growth under mixed mode loading. Int J Solids Struct 1994;31(16):2167–93.
[37] Xu G, Ortiz M. A variational boundary integral equation method for the analysis of 3d cracks of arbitrary geometry modelled as continuous distribution of dislocation loops. Int J Numer Meth Eng 1993;31:3675–701.